http://dx.doi.org/10.21577/0103-5053.20170147

J. Braz. Chem. Soc., Vol. 28, No. 12, 2490-2499, 2017.
Printed in Brazil - ©2017 Sociedade Brasileira de Química
0103 - 5053 $6.00+0.00

Article

The Structure and Composition of Corrosion Product Film and its Relation to Corrosion Rate for Carbon Steels in CO_2 Saturated Solutions at Different Temperatures

Yong Zhou,[a] Pei Zhang,[b] Yu Zuo,[c] Dong Liu[a] and Fuan Yan[a]*

[a]*Key Laboratory for Green Chemical Process of Ministry of Education, Wuhan Institute of Technology, 430205 Wuhan, China*

[b]*Guangxi Key Laboratory of Agricultural Resources Chemistry and Biotechnology, College of Chemistry and Food Science, Yulin Normal University, 537000 Yulin, China*

[c]*Beijing Key Laboratory of Electrochemical Process and Technology for Materials, Beijing University of Chemical Technology, 100029 Beijing, China*

For carbon steels immersed in CO_2 saturated solutions at different temperatures, the structure and the composition of corrosion product film formed on the steel surface were studied by scanning electron microscope (SEM), X-ray diffraction (XRD) and X-ray photoelectron spectroscopy (XPS). The corrosion rate of the steel was evaluated by potentiodynamic polarization, and the relation between the corrosion rate and the film property was discussed. The corrosion rate of the steel was very closely associated with the structure and the composition of corrosion product film, which were affected significantly by the solution temperature. From 30 to 60 °C, the corrosion product film composed of $FeCO_3$ was porous and poorly adherent, and the corrosion rate increased with the rise of temperature. At 70 and 80 °C, the corrosion product film was also composed of $FeCO_3$ and presented a compact and dense cubic crystal structure, resulting in the decrease on the corrosion rate. The corrosion rate increased once again when the temperature was up to 90 °C, which was attributed to the negative effect of high temperature water vapor corrosion on the grain coarsening and the part exfoliation for the $FeCO_3$ film.

Keywords: carbon steel, corrosion product film, CO_2 saturated solution, temperature, corrosion resistance

Introduction

Carbon dioxide (CO_2) corrosion is one of the most typical and universal material corrosion failure for carbon steels in oil and gas industries.[1-3]

At present, studies involving CO_2 corrosion for carbon steels are mainly focused on CO_2 saturated brine in order to simulate actual CO_2 corrosion environments, and the corrosion behavior of carbon steels is mainly dependent on the following factors: temperature, CO_2 partial pressure, aggressive or inhibitive species, pH and flow rate.[4-9] Zhu *et al.*[4] studied the corrosion behavior of the N80 carbon steel in oil field formation water containing CO_2 and reported that the temperature variation played a critical role in the corrosion rate of the N80 steel. The film on the N80 steel surface was mainly composed of iron carbonate ($FeCO_3$). The temperature rise not only accelerated the steel dissolution but also promoted to the formation of $FeCO_3$ film. Further, the authors reported that the addition of acetic acid promoted the cathodic process and inhibited the anodic process. However, the detailed effect of temperature on the microstructure of $FeCO_3$ film was not discussed. Gao *et al.*[5] studied the mechanical property of CO_2 corrosion film and its relationship to the general and localized corrosion rates for the X65 carbon steel in simulated stratum water containing Ca^{2+}, Mg^{2+}, Cl^-, SO_4^{2-} and HCO_3^-. The authors reported that under static conditions from 0.1 to 1.0 MPa CO_2 partial pressure, the film on the X65 steel surface was composed of $FeCO_3$, $MgCO_3$ and $CaCO_3$; under dynamic conditions, the film composition was $FeCO_3$ and $CaCO_3$ mainly. At the same time, the presence of chloride anions induced the initiation of localized corrosion, and the corrosion rates of both the general corrosion and the localized corrosion increased with the increase of flow rate and CO_2 partial pressure. Further,

*e-mail: zhouyong@wit.edu.cn

Gao *et al*.[6] also studied the growth mechanism of CO_2 corrosion film on the X65 steel surface and reported that the crystal growth controlled the formation of $FeCO_3$ film at the initial stage when the relative supersaturation of $FeCO_3$ was low. The nucleation process was accelerated at the high $FeCO_3$ supersaturation, and the high nucleation rate resulted in the formation of relatively compact film. Unfortunately, in the studies of Gao *et al*.,[5,6] the effect of CO_2 corrosion film on the corrosion rate was not discussed in detail. Cui and co-workers[7] studied the chemical composition and the microstructure of CO_2 corrosion film for the N80 steel exposed to simulated stratum water containing $CaCl_2$ 15 g L^{-1} and $NaHCO_3$ 1.1 g L^{-1}. The authors reported that the film was composed of a complex carbonate $FeCO_3$ and $CaCO_3$ and of a limited amount of α-FeOOH mainly. The complex carbonate was unstable and could be partially decomposed to α-FeOOH in dry air. However, the relation between the corrosion rate and the film property was not discussed. Sun *et al*.[8] studied the formation mechanism of CO_2 corrosion film and the electrochemical characteristic of the low alloy steel in CO_2 saturated solution containing Mg^{2+}, Ca^{2+}, Cl^-, SO_4^{2-} and HCO_3^-. The authors reported that the film on the steel surface was composed of $FeCO_3$, $CaCO_3$ and $MgCO_3$, which presented the different formation mechanism. As the main component, the precipitation of $FeCO_3$ might be very closely related to cementite Fe_3C. At the initial stage, the steel substrate dissolved preferentially and left Fe_3C behind, resulting in a high concentration of Fe^{2+} between lamellar Fe_3C. This condition promoted the precipitation of $FeCO_3$ until the whole steel surface was covered by $FeCO_3$. However, the effect of temperature on the precipitation of $FeCO_3$ was not discussed. Yang and co-workers[9] studied the corrosion behavior of the pipeline steel in simulated produced water saturated with supercritical CO_2 and reported that the film on the steel surface, which significantly affected the corrosion behavior of the pipeline steel, was mainly composed of $FeCO_3$, $CaCO_3$ and α-FeOOH. The element distribution of Fe, Ca, C and O was inhomogeneous, and the film formed at a low temperature was more stable than that formed at a high temperature. According to the above reports,[4-9] CO_2 corrosion film on the surface of carbon steels is relatively complicated on the chemical composition and composed of two components mainly: one is the corrosion product composed of $FeCO_3$ attributed to the dissolution of iron element from the carbon steel substrate, and the other is the salt scale composed of $CaCO_3$ and $MgCO_3$ mainly due to the combined action of Ca^{2+}, Mg^{2+} and CO_3^{2-} in CO_2 corrosion environments.

However, CO_2 saturated brine containing Ca^{2+}, Mg^{2+}, Cl^-, HCO_3^- and SO_4^{2-} is very close to the actual component of CO_2 corrosion environments, but it is difficult to study the property of corrosion product film in CO_2 saturated brine. The main reason can be attributed to the following two aspects: the precipitation of salt scale and the occurrence of localized corrosion.[10-15] In contrast, the chemical component of CO_2 saturated solution is relatively simple compared with that of CO_2 saturated brine, in which the effects of salt scale and localized corrosion can be neglected. In this work, the structure and the composition of corrosion product film formed on the surface of carbon steels immersed in CO_2 saturated solutions at different temperatures are studied by scanning electron microscope (SEM), X-ray diffraction (XRD) and X-ray photoelectron spectroscopy (XPS), and the corrosion rate of the steel is evaluated by potentiodynamic polarization test. At the same time, the relation between the corrosion rate and the film property is also discussed in detail.

Experimental

The studied material was Q235 carbon steel with the following chemical composition (wt.%): C, 0.16; Mn, 0.53; Si, 0.30; S, 0.045; P, 0.015; and Fe, 98.95. Specimens were manually abraded up to 1000 grit with SiC abrasive papers, rinsed with de-ionized water and degreased in alcohol. For the electrochemical measurement, the specimens with the dimension of 1 × 1 × 0.3 cm were coated with epoxy resin, leaving 1.0 cm^2 exposed to solution as the working electrode. For the immersion test, the specimens with the dimension of 5 × 1 × 0.3 cm were suspended with PTFE rubber belt completely exposed to the solution.

The studied solution was CO_2 saturated solutions at different temperatures. The pH value and the CO_2 concentration for the studied solution were 3.7 and 0.4 mol L^{-1} analyzed with short range pH paper and by the MT/T 257-2000 standard,[16] respectively. The solution temperature was controlled with an electro-thermostatic water bath.

The potentiodynamic polarization tests were performed using a CS350 electrochemical workstation (China). A typical three electrode system was applied for all the polarization tests. The system was composed of a saturated calomel electrode (SCE) as reference electrode, a platinum sheet as counter electrode and the carbon steel specimen with the dimension of 1 × 1 × 0.3 cm as working electrode. Before each polarization test, the working electrode was immersed in the tested solution for 60 min to ensure the open circuit potential (OCP) to be stable. The potential scanning rate was 0.5 mV s^{-1}, and the potential scanning range was from –0.3 to 0.3 V_{OCP}.

The carbon steel specimens with the dimension of 5 × 1 × 0.3 cm were immersed in CO_2 saturated solutions at different temperatures for 1 h. The cross-sectional

and surface morphologies were observed by a SU1510 SEM instrument (Japan). The surface composition was analyzed by a Kevex SuperDry energy dispersion X-ray spectroscopy (EDS) instrument attached on the SEM system, a D8-Advance XRD instrument (Germany) and an ESCALAB-250 XPS instrument (USA).

Results and Discussion

Cross-sectional microstructure

Figure 1 shows the cross-sectional SEM morphologies of the carbon steel specimens immersed in CO_2 saturated solutions at different temperatures for 1 h. There is a continuous and intact film on the surface of each specimen. However, the effect of temperature on the film microstructure is very prominent. Table 1 shows the relative atom abundance of Fe, C and O in the surface film formed on the specimen surface immersed in CO_2 saturated solutions at different temperatures by EDS analysis.

From Figure 1a, for the specimen immersed in the solution at 30 °C, a film with the average thickness about 0.78 μm is observed on the specimen surface. EDS analysis revealed that Fe, C and O were present in the film, and the relative atom abundance of Fe, C and O is, respectively, 19.37, 18.82 and 61.81% (shown in Table 1), which is very close to 1:1:3, suggesting that the film formed at 30 °C is mainly composed of $FeCO_3$. Nesic *et al.*[1,17,18] reported that when carbon steels were exposed in CO_2 corrosion environments, the formation of CO_2 corrosion film was dominated by the following two reverse processes: the precipitation process and the undermining process. At low temperature, the kinetics of undermining process was faster than that of precipitation process, resulting in that a porous and non-protective film was obtained on the surface of carbon steels.[1] At the same time, Schmitt[19] and Dugstad *et al.*[20] reported that when the temperature was less than 70 °C, the corrosion product film was porous as well as poorly adherent and could not provide the effective corrosion resistance for the steel substrate. Similar results

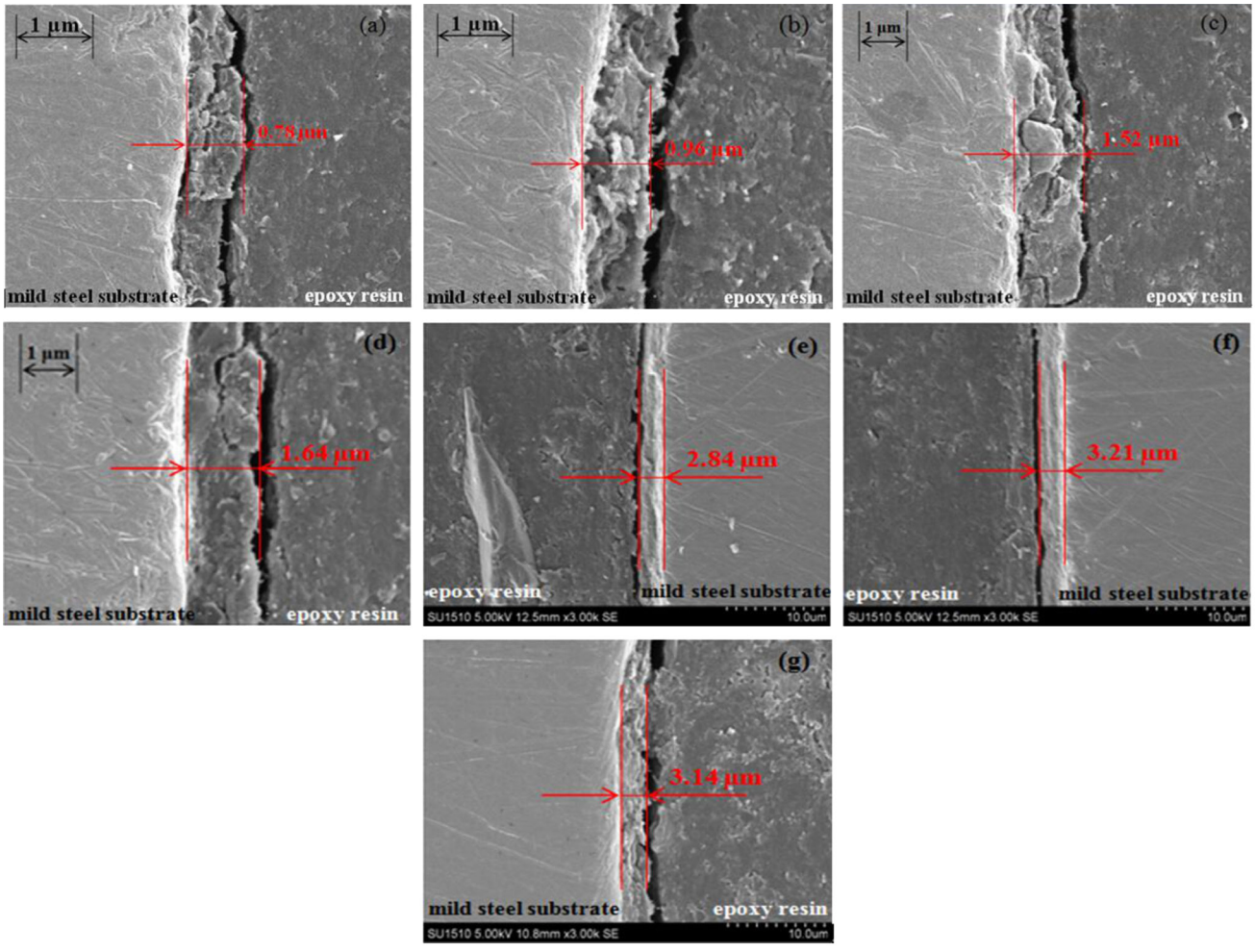

Figure 1. Cross-sectional SEM morphologies of carbon steel specimens immersed in CO_2 saturated solutions for 1 h at different temperatures: (a) 30, (b) 40, (c) 50, (d) 60, (e) 70, (f) 80 and (g) 90 °C.

Table 1. Relative atom abundance of Fe, C and O in surface film formed on specimen surface immersed in CO_2 saturated solutions at different temperatures by EDS analysis

Temperature / °C	Fe / %	C / %	O / %
30	19.37	18.82	61.81
40	20.17	19.92	59.91
50	20.61	19.73	59.66
60	19.87	20.21	59.92
70	20.73	19.25	60.02
80	19.27	20.15	60.58
90	32.92	10.27	56.81

are also observed in the present study. From Figure 1a, there are some cracks and pores within the $FeCO_3$ film, and the presence of gap between the $FeCO_3$ film and the Q235 substrate is observed, indicating that the $FeCO_3$ film formed at 30 °C is poorly compact and adherent. From Figures 1b to 1d, the microstructure of the film formed from 40 to 60 °C is similar to that of the film formed at 30 °C: the presence of cracks, pores and gaps is also observed. Further, from the results of EDS shown in Table 1, the film formed from 40 to 60 °C is also composed of $FeCO_3$. Besides, Figure 1 also illustrates that the film thickness increases slightly with the rise of temperature from 30 to 60 °C, which will be discussed in detail later.

From Figure 1e, for the specimen immersed in the solution at 70 °C, a compact and dense film with the average thickness about 2.84 μm is observed on the specimen surface. EDS analysis revealed that the main composition of the film is also $FeCO_3$, as shown in Table 1. Compared with the microstructure of the $FeCO_3$ film formed at the low temperature, for the $FeCO_3$ film formed at 70 °C, there is no pore and crack within the $FeCO_3$ film and no gap between the $FeCO_3$ film and the Q235 substrate, indicating the good corrosion resistance. From Figure 1f, the film formed at 80 °C is similar to that formed at 70 °C, which is also composed of $FeCO_3$ according to the EDS results shown in Table 1.

For the specimen immersed in the solution at 90 °C, as shown in Figure 1g, although the microstructure of the film formed at 90 °C is also similar to that of the film formed at 70 or 80 °C, EDS analysis revealed that the relative atom ratio of Fe, C and O is far away from 1:1:3 shown in Table 1, suggesting that the composition of the film formed at 90 °C may be complicated in comparison with that of the film formed at the low temperature, which will be confirmed by XRD and XPS later.

Film thickness

Figure 2 shows the effect of temperature on the thickness for the corrosion product film formed on the specimen surface immersed in CO_2 saturated solutions at different temperatures for 1 h, where each datum is the average value of ten randomly selected sites at the surface film on the cross-sectional SEM morphology, and the error ranges are also shown. From Figure 2, the film thickness increases slightly with the rise of temperature from 30 to 60 °C. Afterwards, the film thickness shows very sharp increase from 1.64 to 2.84 μm between 60 and 70 °C. Finally, when the temperature is up to 70 °C, the film thickness shows slight variation with the rise of temperature.

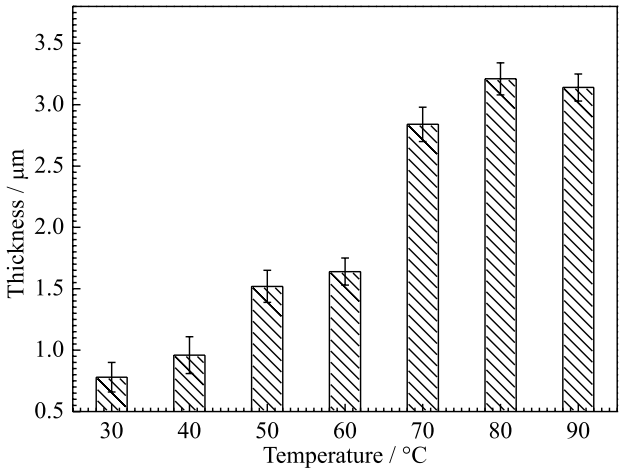

Figure 2. Effect of temperature on thickness for corrosion product film formed on specimen surface immersed in CO_2 saturated solutions at different temperatures for 1 h.

The thickness variation of corrosion product film may be attributed to the effect of temperature on the solubility product constant (K_{sp}) and the solubility temperature coefficient.[21-23] Nesic and co-workers[21] studied the effects of temperature and ionic strength on the solubility limit of iron carbonate. The authors reported that the K_{sp} value of $FeCO_3$ could be described as follows:

$$\log K_{sp} = -59.3498 - 0.041377 \times T_k - 2.1963 / T_k + 24.5724 \times \log T_k + 2.518 \times I^{0.5} - 0.657 \times I \quad (1)$$

According to the above equation, the K_{sp} value decreases with the rise of temperature, which is consistent with the experimental results.[21] Waard *et al.*[23] reported that the solubility temperature coefficient of $FeCO_3$ showed a negative value, indicating that the solubility of $FeCO_3$ decreased with the rise of temperature. Therefore, it can be inferred that the $FeCO_3$ crystal formed at the high temperature is more stable than that formed at the low temperature. On the other hand, it was reported that the undermining process and the precipitation process owned the different temperature susceptibility.[1,17,18] At high

temperature, the kinetics of precipitation process could be accelerated quickly and was more prominent than that of undermining process,[1] which is also favorable for the formation of corrosion product film. The above two aspects can be responsible for the thickness variation of corrosion product film.

Surface microstructure

Figure 3 shows the surface SEM morphologies of the carbon steel specimens immersed in CO_2 saturated solutions at different temperatures for 1 h. Like the results of cross-sectional microstructure shown in Figure 1, Figure 3 illustrates that the effect of temperature on the crystal structure of $FeCO_3$ is also prominent.

From Figures 3a to 3d, for the specimens immersed in the solutions from 30 to 60 °C, there is no obvious crystal shape on the specimen surface, whereas some scratches due to mechanical action of abrasive paper are observed. On the other hand, EDS analysis revealed that the relative atom abundance of Fe for the four specimens was more than 60%. The above results indicate that the $FeCO_3$ film formed at the low temperature is relatively thin, which is in agreement with the results of cross-sectional SEM morphology. It was reported that when the temperature was low, the negative effect of undermining process were prominent compared with the positive effect of precipitation process,[1,17,18] which is adverse to the formation of CO_2 corrosion film.

However, for the specimens immersed in the solutions at 70 and 80 °C shown in Figures 3e and 3f, the surface microstructure of $FeCO_3$ film shows an obvious cubic crystal shape. Gao *et al.*[5,6,24] reported that the corrosion product film consisted of cubic crystals provided good corrosion resistance for the steel substrate against CO_2 corrosion. Zhu *et al.*[4] also reported that the cubic structure could effectively resist the diffusion/permeation of aggressive species reaching the film/substrate interface. Further, for the specimen immersed in the solution at 70 °C, EDS analysis revealed that Fe, C and O were present in the film, and the relative atom abundance of Fe, C and O was

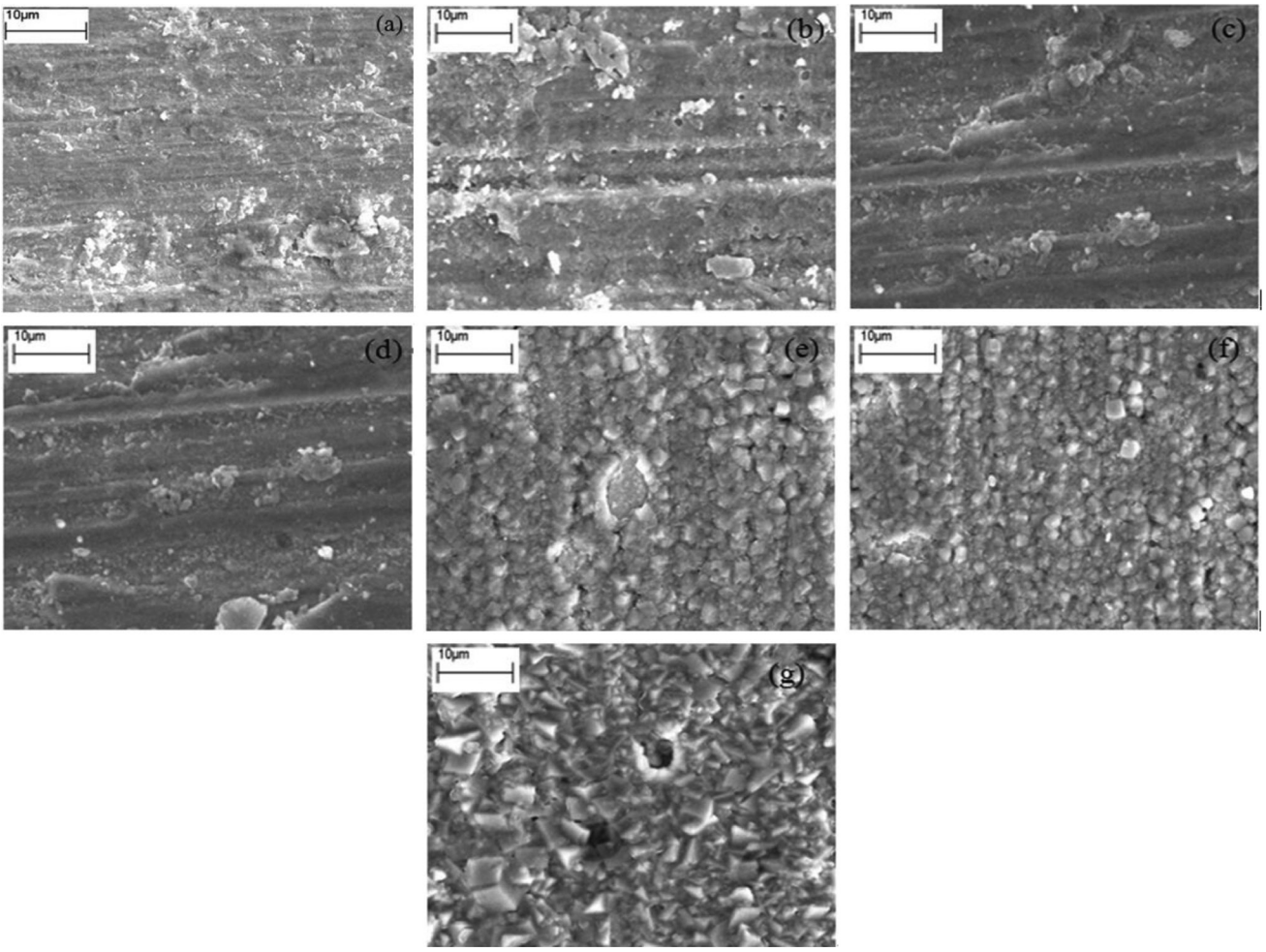

Figure 3. Surface SEM morphologies of carbon steel specimens immersed in CO_2 saturated solutions for 1 h at different temperatures: (a) 30, (b) 40, (c) 50, (d) 60, (e) 70, (f) 80 and (g) 90 °C.

19.63, 20.16 and 60.21%, respectively. The relative atom ratio of Fe, C and O is approximately 1:1:3, suggesting that the thickness of $FeCO_3$ film formed at 70 °C increases compared with that of $FeCO_3$ film formed from 30 to 60 °C, which is consistent with the results shown in Figure 2.

From Figure 3g, for the specimen immersed in the solution at 90 °C, the surface film also shows the cubic crystal structure. However, the crystals formed at 90 °C are obviously more coarse and bulky than those formed at 70 or 80 °C. It was reported that the surface film consisted of exquisite crystals could provide better corrosion resistance than that consisted of coarse crystals,[25] indicating that the corrosion rate of the steel in the solution at 90 °C is higher than that of the steel in the solution at 70 or 80 °C. Later, the relation between the film property and the corrosion rate will be discussed.

Film composition

Figure 4 shows the XRD patterns of the carbon steel specimens immersed in CO_2 saturated solutions at different temperatures for 1 h. For the specimens immersed in the solutions from 30 to 60 °C, there are only three main peaks visible on the patterns at about 45°, 65° and 82°, corresponding to α-Fe. However, the above XRD results seem to contradict the results of SEM and EDS shown in Figure 1 and Table 1: the $FeCO_3$ film has been formed but cannot be detected by XRD analysis. Because the measuring depth of XRD is beyond 10 μm, the $FeCO_3$ film formed from 30 to 60 °C is too thin to be detected. For the specimens immersed in the solutions at 70 and 80 °C, besides three diffraction peaks at 45°, 65° and 82°, other three diffraction peaks at about 24°, 32° and 53° corresponding to $FeCO_3$ were detected by XRD analysis, suggesting that the $FeCO_3$ film formed at the high temperature is thicker than that formed at the low temperature. However, for the specimen immersed in the solution at 90 °C, the diffraction peaks at 24° and 53° become no obvious, and the diffraction peak at 32° moves a little to the low angle direction, which may be due to the composition of the film formed at 90 °C is more complicated than that of the film formed from 30 to 80 °C.

Figure 5 shows the wide-scan XPS spectrum of the carbon steel specimen immersed in CO_2 saturated solution at 30 °C for 1 h. There are three main peaks visible on the spectrum at about 711, 531 and 285 eV corresponding, respectively, to Fe 2p, O 1s and C 1s. The XPS result provides evidence for the presence of Fe, C and O, which is in agreement to the results of EDS and XRD. The wide-scan XPS spectra of the specimens immersed in the solutions from 40 to 90 °C are similar to that of the

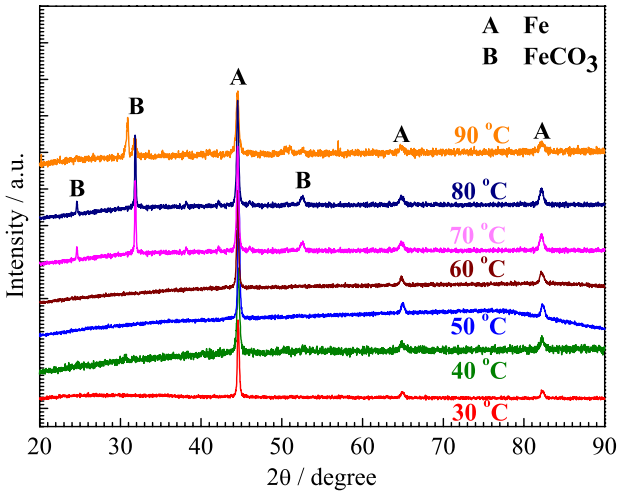

Figure 4. XRD patterns of carbon steel specimens immersed in CO_2 saturated solutions at different temperatures for 1 h.

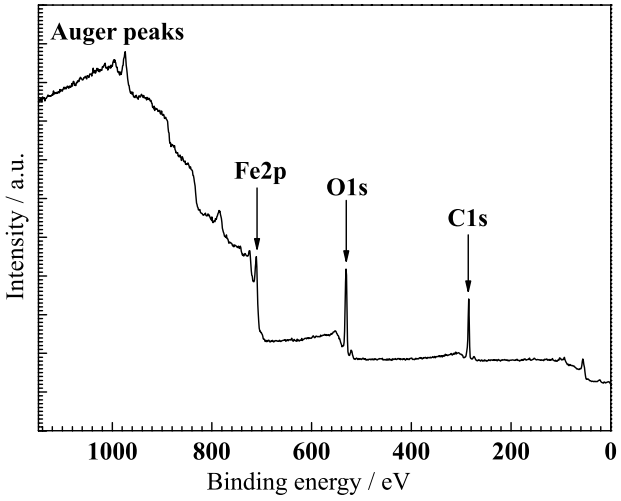

Figure 5. Wide-scan XPS spectrum of carbon steel specimen immersed in CO_2 saturated solution at 30 °C for 1 h.

specimen immersed in the solution at 30 °C: only Fe 2p, C 1s and O 1s were detected by XPS analysis.

Figure 6 shows the high-resolution XPS spectra of Fe 2p for the carbon steel specimens immersed in CO_2 saturated solutions at 30 and 90 °C for 1 h. Table 2 summarizes the reported binding energy values for Fe 2p in various model compounds from literature.

According to the reported data in Table 2, for the specimen immersed in the solution at 30 °C, the Fe 2p spectrum reveals two peaks at 711.70 and 709.70 eV, corresponding to Fe element in α-FeOOH and $FeCO_3$, respectively. The high-resolution XPS spectra of Fe 2p for the specimens immersed in the solutions from 40 to 80 °C are similar to that for the specimen immersed in the solution at 30 °C: only the presence of α-FeOOH and $FeCO_3$ was detected by XPS analysis. In contrast, for the specimen immersed in the solution at 90 °C, the high-resolution

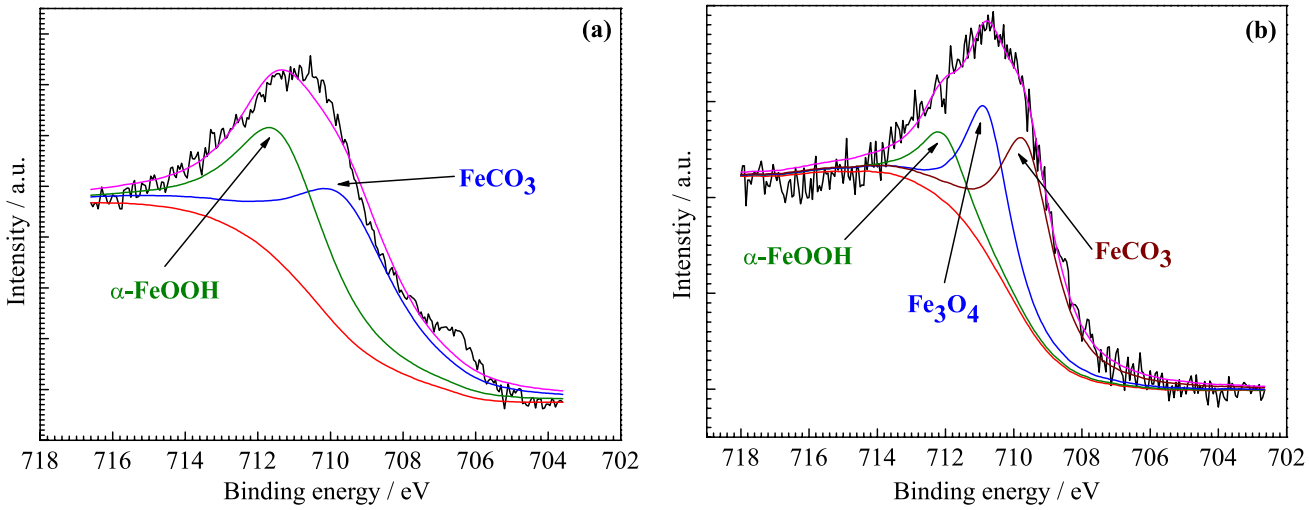

Figure 6. High-resolution XPS spectra of Fe 2p for carbon steel specimens immersed in CO_2 saturated solutions for 1 h at (a) 30 and (b) 90 °C.

Table 2. Reported binding energy values for Fe 2p in various model compounds from literature

Species	Binding energy /eV	Reference
α-FeOOH	711.83	7
	711.80	26,27
	711.65	9
	711.38	7
	711.00	28
Fe_3O_4	710.90	29
	710.80	29
	710.40	30
$FeCO_3$	709. 75	7
	709.67	7
	709.60	31
	709.52	9

XPS spectrum of Fe 2p is obvious different, as shown in Figure 6b. The Fe 2p spectrum reveals three peaks at 711.95, 710.90 and 709.80 eV, respectively corresponding to Fe element in α-FeOOH, Fe_3O_4 and $FeCO_3$.

$FeCO_3$ is the carbonate corrosion product for carbon steels exposed to CO_2 corrosion environments, and the mechanism for the precipitation of $FeCO_3$ is as follows:[4,32]

$$Fe^{2+} + CO_3^{2-} \rightarrow FeCO_3 \quad (2)$$

$$Fe^{2+} + 2HCO_3^{-} \rightarrow Fe(HCO_3)_2 \quad (3)$$

$$Fe(HCO_3)_2 \rightarrow FeCO_3 + CO_2 + H_2O \quad (4)$$

For α-FeOOH, Heuer and Stubbins[27] reported that the exposure of $FeCO_3$ to air could result in hydrolysis and oxidation to FeO/FeOOH. Cui and co-workers[7] reported that the presence of α-FeOOH was attributed to the temporary storage of the tested specimen in desiccated air before XPS analysis. Similar results are also reported by Zhao and Chen[26] and Zhou and Zuo.[33] Fe_3O_4 is the oxide corrosion product for iron-based metal materials exposed to high temperature water vapor environments, and the formation mechanism of Fe_3O_4 is as follows:[34,35]

$$3Fe + 4H_2O\ (g) \rightarrow Fe_3O_4 + 4H_2\ (g) \quad (5)$$

Electrochemical behavior

Figure 7 shows the polarization curves of the carbon steel specimens in CO_2 saturated solutions at different temperatures. Regardless of the solution temperature, all of the specimens presented the electrochemical characteristic of active dissolution in the tested electrolyte. However, the effect of temperature on the corrosion current density (i_{corr}) is very prominent, as shown in Figure 7.

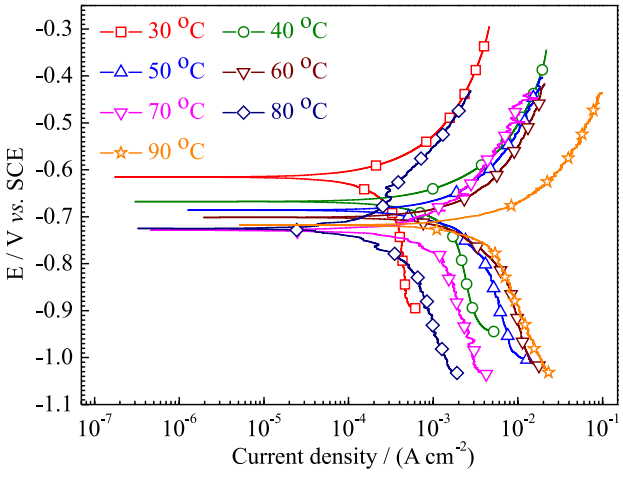

Figure 7. Polarization curves of carbon steel specimens in CO_2 saturated solutions at different temperatures.

From the values of i_{corr}, the corrosion rate (V_L) can be calculated according to the following equations:

$$V_{corr} = (A \times i_{corr} \times 10^4) / (n \times F) \quad (6)$$
$$V_L = (8.76 \times V_{corr}) / \rho \quad (7)$$

In the above two equations, A represents the relative atomic weight (g), A = 56 g; i_{corr} represents the corrosion current density (A cm^{-2}), which can be obtained from Figure 7; n represents the chemical valence, n = 2; F represents the Faraday constant (A h), F = 96500 C = 26.8 A h; V_{corr} represents the weight corrosion rate (g m^{-2} h^{-1}), which can be calculated by equation 6; ρ represents the material density (g cm^{-3}), ρ = 7.8 g cm^{-3}; V_L represents the corrosion rate (mm y^{-1}), which can be calculated by equation 7.

Relation between corrosion rate and corrosion product film

Figure 8 shows the effect of temperature on the corrosion rate for the carbon steel specimens immersed in CO_2 saturated solutions, where each datum is the average value of five parallel polarization tests, and the error ranges are also shown. From Figure 8, the corrosion rate increases gradually with the rise of temperature from 30 to 60 °C and shows a peak value at 60 °C. However, when the temperature is up to 70 °C, the corrosion rate decreases and shows a least value at 80 °C. Finally, the corrosion rate increases once again when the temperature is 90 °C.

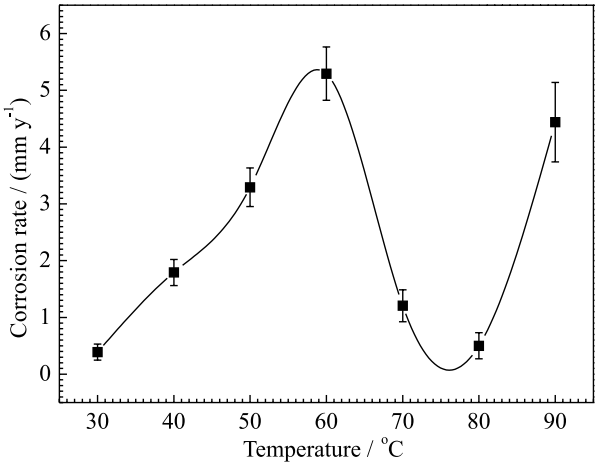

Figure 8. Effect of temperature on corrosion rate for carbon steel specimens in CO_2 saturated solutions.

From the above results of SEM, XRD and XPS, a corrosion product film with different structure and composition is formed on the steel surface when the studied steel is exposed in CO_2 saturated solution, and the property of corrosion product film is affected significantly by the solution temperature. It is generally accepted that the corrosion behavior of carbon steels in CO_2 corrosion environments is very closely associated with the presence of corrosion product film.[17,18,24] The relation between the corrosion rate and the film property is discussed as follows.

It was reported that the corrosion resistance of CO_2 corrosion film was mainly attributed to its role of mechanical barrier to restrain the diffusion/permeation of aggressive species reaching the substrate surface, so a protective film should have very few film defects.[5,6] Because of the different temperature susceptibility between the precipitation process and the undermining process, at low temperature, the undermining rate was usually faster than the precipitation rate, resulting in that the undermining process controlled the film-formed kinetics on the surface of carbon steels.[17,18] In this case, a porous, poorly adherent and non-protective film would be obtained on the steel surface, and the film was almost no diffusion/permeation resistance to restrain the cathodic species, such as H^+, H_2O and H_2CO_3, reaching the film/substrate interface.[1] The corrosion rate was dominated by the electrochemical step, and the following cathodic reactions occurred on the steel surface readily:[36-40]

$$H^+ + e \rightarrow H \quad (8)$$
$$H_2O + e \rightarrow H + OH^- \quad (9)$$
$$H_2CO_3 + e \rightarrow H + HCO_3^- \quad (10)$$

In this work, from 30 to 60 °C, although the thickness of $FeCO_3$ film increases with the rise of temperature as shown in Figure 2, the presence of pores and cracks within the $FeCO_3$ film and the presence of gap between the $FeCO_3$ film and the Q235 substrate are observed, as shown in Figure 1, indicating that the $FeCO_3$ film formed from 30 to 60 °C cannot provide the good physical barrier to the steel substrate. At the same time, Nesic *et al.*[38] reported that the kinetics of cathodic reactions was accelerated significantly with the rise of temperature from 20 to 80 °C. Ogundele and White[39] reported the similar results on the cathodic kinetics in the temperature range from 25 to 95 °C. Therefore, in this work, the increased corrosion rate from 30 to 60 °C is attributed to the combined effects of temperature and non-protective $FeCO_3$ film.

However, with the rise of temperature, the high temperature accelerated the kinetics of precipitation process, and the precipitation rate would exceed the undermining rate, resulting in a dense, compact and protective film formed on the surface of carbon steels.[17,18] In the present study, similar results are also observed in Figures 1 and 3. From Figures 1e and 1f, there is no pore and crack within the $FeCO_3$ film and no gap between the $FeCO_3$ film and the Q235 substrate, indicating the good

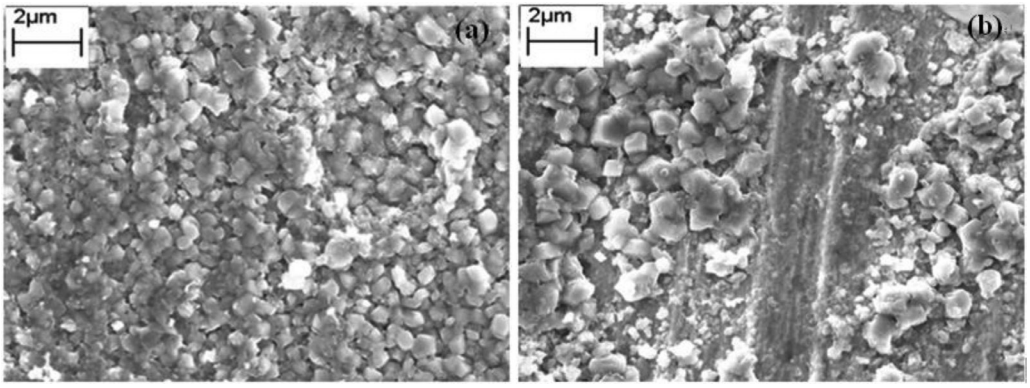

Figure 9. Enlarged surface SEM morphologies of carbon steel specimens immersed in CO_2 saturated solutions for 1 h at (a) 80 and (b) 90 °C.

function of mechanical barrier for the $FeCO_3$ film. On the other hand, from Figures 3e and 3f, the $FeCO_3$ film shows the cubic crystal structure, which can effectively restrain the diffusion/permeation of aggressive species to the film/substrate interface. In this case, the reactant supply for electrochemical reactions shown in equations 8 to 10 become more difficult, and the corrosion rate is dominated by the step of mass transfer. Therefore, the decreased corrosion rate at 70 to 80 °C is due to the protective $FeCO_3$ film. Besides, the fact that the corrosion rate at 80 °C is slightly lower than that at 70 °C may be attributed to that the $FeCO_3$ film formed at 80 °C is thicker than that formed at 70 °C, as shown in Figure 2.

The composition and the structure of corrosion product film formed at 90 °C are obviously different from those of $FeCO_3$ film formed from 30 to 80 °C. Figure 6b illustrates that the signal of Fe_3O_4 was detected by XPS analysis. However, according to the XRD result for the specimen immersed in the solution at 90 °C, except the diffraction peaks corresponding to α-Fe and $FeCO_3$, no peak corresponding to Fe_3O_4 was detected by XRD analysis, suggesting the content of Fe_3O_4 on the steel surface is relatively few. The presence of a small amount of Fe_3O_4 can increase the relative atom abundance of Fe and decrease the corresponding values of C and O, which is consistent with the EDS results shown in Table 1. Therefore, it can be inferred that the corrosion product film formed at 90 °C is composed mainly of $FeCO_3$ and of a small amount of Fe_3O_4. The presence of Fe_3O_4 is attributed to the occurrence of high temperature water vapor corrosion.[34,35] Further, Han *et al.*[34] reported that a limited amount of Fe_3O_4 was distributed discontinuously between the $FeCO_3$ film and the steel substance. Figure 9 shows the enlarged surface SEM morphologies of the carbon steel specimens immersed in CO_2 saturated solutions at 80 to 90 °C for 1 h.

Comparing Figures 9a and 9b, the cubic crystals formed at 90 °C are more coarse and bulky than those formed at 80 °C, indicating that the corrosion resistance of the film formed at 80 °C is greater than that of the film formed 90 °C. On the other hand, from Figure 9b, some cubic crystals have been peeled off from the steel surface, which is also attributed to the presence of Fe_3O_4 on the steel surface. According to the report of Han *et al.*,[34] the discontinuous Fe_3O_4 film not only could not provide the corrosion resistance for the steel substrate but also decreased the adhesive force of $FeCO_3$ film to the steel surface. Therefore, the increased corrosion rate at 90 °C is attributed to the combined effects of the grain coarsening and the part exfoliation on the $FeCO_3$ film, which is derived from the occurrence of high temperature water vapor corrosion.

Conclusions

In this work, the relation between the evolution of corrosion rate and the property of corrosion product film for carbon steels immersed in CO_2 saturated solutions at different temperatures was studied and discussed. The corrosion rate of the studied steel was very closely related to the structure and the composition of corrosion product film, which were affected significantly by the solution temperature. From 30 to 60 °C, the corrosion product film composed of $FeCO_3$ was porous and poorly adherent, and the corrosion rate increased with the rise of temperature. At 70 and 80 °C, the corrosion product film was also composed of $FeCO_3$ and showed a compact and dense cubic crystal structure, resulting in the decrease on the corrosion rate. The corrosion rate increased once again when the temperature was up to 90 °C, which was attributed to the negative effect of high temperature water vapor corrosion on the grain coarsening and the part exfoliation for the $FeCO_3$ film.

Acknowledgments

This work is supported by the National Nature Science Foundation of China (contract 51601133, 51210001 and 51401150).

References

1. Nesic, S.; *Corros. Sci.* **2007**, *49*, 4308.
2. Usher, K. M.; Kaksonen, A. H.; Bouquet, D.; Cheng, K. Y.; Geste, Y.; Chapman, P. G.; Johnston, C. D.; *Corros. Sci.* **2015**, *98*, 354.
3. Nesic, S.; Nordsveen, M.; Maxwell, N.; Vrhovac, M.; *Corros. Sci.* **2001**, *43*, 1373.
4. Zhu, S. D.; Fu, A. Q.; Miao, J.; Yin, Z. F.; Zhou, G. S.; Wei, J. F.; *Corros. Sci.* **2011**, *53*, 3156.
5. Gao, K. W.; Yu, F.; Pang, X. L.; Zhang, G. A.; Qiao, L. J.; Chu, W. Y.; Lu, M. X.; *Corros. Sci.* **2008**, *50*, 2796.
6. Gao, M.; Pang, X.; Gao K.; *Corros. Sci.* **2011**, *53*, 557.
7. Wu, S. L.; Cui, Z. D.; He, F.; Bai, Z. Q.; Zhu, S. L.; Yang, X. J.; *Mater. Lett.* **2004**, *58*, 1076.
8. Sun, J. B.; Zhang, G. A.; Liu, W.; Lu, M. X.; *Corros. Sci.* **2012**, *57*, 131.
9. Cui, Z. D.; Wu, S. L.; Zhu, S. L.; Yang, X. J.; *Appl. Surf. Sci.* **2006**, *252*, 2368.
10. Xiong, Q. Y.; Zhou, Y.; Xiong, J. P.; *Int. J. Electrochem. Sci.* **2015**, *10*, 8454.
11. Ko, M.; Ingham, B.; Laycock, N.; Williams, D. E.; *Corros. Sci.* **2015**, *90*, 192.
12. Farelas, F.; Galicia, M.; Brown, B.; Nesic, S.; Castaneda, H.; *Corros. Sci.* **2010**, *52*, 509.
13. Fatah, M. C.; Ismail, M. C.; Ari-Wahjoedi, B.; Kuinia, K. A.; *Mater. Chem. Phys.* **2011**, *127*, 347.
14. Zhang, Y. C.; Pang, X. L.; Qu, S. P.; Li, X.; Gao, K. W.; *Corros. Sci.* **2012**, *59*, 186.
15. Zhou, Y.; Yan, F. A.; *Int. J. Electrochem. Sci.* **2016**, *11*, 3976.
16. MT/T 257-2000, *Determination of Free Carbon Dioxide in Coal Mine Water*, The Coal Industry Standard of the People's Republic of China, Beijing, 2000-2001.
17. Nesic, S.; Lee, K. L. J.; *Corrosion* **2003**, *59*, 616.
18. Nesic, S.; Solvi, G. T.; Enerhaug, J.; *Corrosion* **1995**, *51*, 773.
19. Schmitt, G.; *Corrosion* **1991**, *47*, 285.
20. Dugstad, A.; Hemmer, H.; Seiersten, M.; *Corrosion* **2001**, *57*, 369.
21. Sun, W.; Nesic, S.; Woollam, R. C.; *Corros. Sci.* **2009**, *51*, 1273.
22. Smith, H. J.; *J. Am. Chem. Soc.* **2002**, *40*, 879.
23. Waard, C. D.; Lotz, U.; Milliams, D. E.; *Corrosion* **1991**, *47*, 976.
24. Li, T.; Yang, Y. J.; Gao, K. W.; Lu, M. X.; *J. Univ. Sci. Technol. Beijing* **2008**, *15*, 702.
25. Li, Q.; Xu, S. Q.; Hu, S. Y.; Zhang, S. Y.; Zhong, X. K.; Yang, X. K.; *Electrochim. Acta* **2010**, *55*, 887.
26. Zhao, J. M.; Chen, G. H.; *Electrochim. Acta* **2012**, *69*, 247.
27. Heuer, J. K.; Stubbins, J. F.; *Corros. Sci.* **1999**, *41*, 1231.
28. Zhang, J.; Wang, Z. L.; Wang, Z. M.; Han, X.; *Corros. Sci.* **2012**, *65*, 397.
29. Wilson, D.; Langell, M. A.; *Appl. Surf. Sci.* **2014**, *303*, 6.
30. Wang, J. Q.; Wu, W. H.; Feng, D. M.; *Electron Spectroscopy (XPS/XAES/UPS) Introduction*; National Defence Industry Press: Beijing, China, 1992.
31. Lopez, D. A.; Schreiner, W. H.; Sanchez, S. R.; Simison, S. N.; *Appl. Surf. Sci.* **2004**, *236*, 77.
32. Linter, B. R.; Burstein, G. T.; *Corros. Sci.* **1999**, *41*, 117.
33. Zhou, Y.; Zuo, Y.; *J. Electrochem. Soc.* **2015**, *162*, C47.
34. Han, J. B.; Nesic, S.; Yang, Y.; Brown, B. N.; *Electrochim. Acta* **2011**, *56*, 5396.
35. Cheng, Y. F.; Steward, F. R.; *Corros. Sci.* **2004**, *46*, 2405.
36. Xiong, Q. Y.; Xiong, J. P.; Zhou, Y.; Yan, F. A.; *Int. J. Electrochem. Sci.* **2017**, *12*, 4238.
37. Mishra, B.; Hassan, S. A.; Olson, D. L.; Salama, M. M.; *Corrosion* **1997**, *53*, 852.
38. Nesic, S.; Postlethwaite, J.; Olsen, S.; *Corrosion* **1996**, *52*, 280.
39. Ogundele, G. I.; White, W. E.; *Corrosion* **1986**, *42*, 71.
40. Waaed, C. D.; Milliams, D. E.; *Corrosion* **1975**, *31*, 177.

Submitted: June 14, 2017
Published online: August 16, 2017